A VARIATIONAL MODEL FOR OBJECT SEGMENTATION USING BOUNDARY INFORMATION AND STATISTICAL SHAPE PRIOR DRIVEN BY THE MUMFORD-SHAH FUNCTIONAL

Xavier Bresson, Pierre Vandergheynst and Jean-Philippe Thiran

Signal Processing Institute (ITS),
Swiss Federal Institute of Technology (EPFL)
CH-1015 Lausanne, Switzerland
Email: {Xavier.Bresson, Pierre.Vandergheynst, JP.Thiran}@epfl.ch

ABSTRACT

In this paper, we propose a variational model for object segmentation using the active contour method, a geometric shape prior and the Mumford-Shah functional. We propose an energy functional composed by three terms: the first one is based on image gradient, which detects edges, the second term constrains the active contour to get a shape compatible with a statistical model of the target shape, which provides robustness against missing shape information due to cluttering, occlusion and gaps, and the third part drives globally the shape prior towards a homogeneous intensity region. The minimization of the functional gives a system of coupled ordinary and partial differential equations which steady state, computed in a level set framework, provides the solution of the segmentation problem. We mathematically justify our segmentation variational model by proving the existence of a solution minimizing the energy functional in the space of functions of bounded variation. Applications of the proposed model are presented on various synthetic and real-world images.

1. INTRODUCTION AND MOTIVATIONS

During the last decade, variational methods and partial differential equations (PDEs) have been more and more employed to analyse, understand and exploit properties of images in order to design powerful application techniques. Variational methods formulate an image processing or computer vision problem as an optimization problem depending on the unknown variables (which are functions) of the problem. When the optimization functional is differentiable, the calculus of variations provides a tool to find the extremum of the functional leading to a PDE whose steady state gives the solution of the imaging or vision problem. Variational methods and PDEs are well established domains of functional analysis which can offer strong frameworks to correctly formulate image problems. A very attractive property of these mathematical frameworks is to state well-posed problems to guarantee existence, uniqueness and regularity of solutions. Successful mathematical frameworks of functional analysis in computer vision are the theory of viscosity solutions [1] and the framework of functions of bounded variation [2, 3] which have given powerful tools to mathematically justify solutions of many image problems. Finally, applications of variational methods and PDEs have produced a lot of literature in image processing, computer vision and computer graphics as one can read in several books [4, 5, 6, 7, 8].

In computer vision, shape analysis is a core component towards automated vision systems. It can be decomposed into several research domains including shape modeling, shape registration, segmentation and pattern recognition. Among these research aeras, image segmentation plays an important role in computer vision since it is often the basis to many applications. Image segmentation has the global objective of determining the *semantically* important regions in images. In the variational framework, it is solved by two approaches: the Mumford-Shah model and the active contour method. The first one aims at finding a partition of an image into its constituent parts, which is realized by minimizing the Mumford-Shah functional [9], and the second one detects more specific parts using the model of active contours/snakes/propagating interfaces [10]. See Figure 1 as an example of segmentation. Active contour method is a powerful technique to perform segmentation of natural structures. Initially proposed by Kass *et al.* [10], active contours are evolving curves/surfaces (represented by PDEs) under a field of forces, depending on image features and

(a) original image (b) segmented image (c) initial active contour (d) final active contour

Fig. 1. In the variational framework, image segmentation can be realized with the Mumford-Shah functional (a),(b) and the active contours method (c),(d)

intrinsic curve properties, that leads to the minimization of an objective functional. The numerical solution of PDEs in the context of propagating contours uses the powerful technique of level sets whose theoritical fundations are presented by Osher and Sethian in [11]. Level set methods are suitable for evolving interfaces since they are parameter-free and can deal with topological changes. Segmentation performances of fine real-world shapes such as medical structures [12, 13, 14] are remarquable with the level set active contours since they evolve locally (due to PDEs) to globally optimize the functional (the variational model). However, this attractive advantage is also the weakness of the first-generation snakes in presence of noise and bad image contrast as they can lead to bad segmentation results of important regions. To overcome this drawback, some authors have incorporated region-based evolution criteria into active contours, built from statistics and homogeneous intensity requirements [15, 16, 17, 18, 19, 20]. However the segmentation of *structures of interest* with these second-generation active contours gives bad outcomes in the presence of occlusions and strongly cluttered background. Therefore the integration in the segmentation task of prior shape knowledge about the region to segment was naturally proposed as a solution to overcome these problems.

The geometric shape prior of regions to be extracted can be defined by different models such as Fourier descriptors, medial axis or atlas-based parametric models. A performant shape representation has to capture all natural variations, be invariant with respect to spatial transformations and compact to reduce the number of model parameters. A solution consists in using a set of training shapes of object of interest and look for a compact representation which can best represent the training set. Shape models based on this idea are built on statistics such as the principal components analysis (PCA) [21, 22, 23, 24]. Recently, the level set representation of shapes, used in the active contours framework, has been employed as shape modeling [22, 23, 24]. Level set modeling presents some strong properties in shape description. Firstly, it is an implicit and intrinsic representation and as previously said, it is independant of the contour parametrization and can deal with topological changes. This shape model can represent shapes of any intrinsic dimensions such as curves, surfaces and hyper-surfaces. Then, it also provides a natural way to estimate shape geometric properties such as the curvature and the normal to contours. Level set functions are often represented by signed distance functions (SDFs) defined on the image space where the shape information is propagated in the normal direction in such a way that the shape produces similar shapes (iso-contours/isophotes) consistently aligned in the image domain. Finally, this shape representation is coherent with the level set variational model of evolving contours so that it can be naturally integrate in the active contours framework.

The integration of a geometric shape model in the segmentation process can be realized with a shape registration method to map the prior shape onto the snake shape (the target shape) as done in [22, 25, 23]. The shape registration problem consists in determining a geometric deformation field (rigid, affine, non-rigid) between a reference shape and a target shape which optimizes a shape correspondance criterion. In [22], Leventon *et al.* have employed level set representations of the prior shape and the active contours and they have registered both shapes by maximizing a similarity measure between the two level sets. They have observed that the level set representation improves the registration, both in terms of robustness and accuracy. The main reason is that the contour point-wise correspondance problem is replaced by a grid point-wise intensity correspondance problem between the level set surfaces representing the prior shape and the snake.

The objective of this paper is to propose a segmentation method for extracting structures of interest whose global shape is a priori known thanks to a statistical model. For the reasons previously described, we will use an implicit/level set representation of shapes and employ a compact model to represent shapes of a training set. The model developed by Leventon *et al.*, based on the principal components analysis of training shapes represented by level set functions, appears to fulfil our shape model conditions. Indeed, this linear model allows us to represent *global shape variations* of a training family of a structure of interest. This shape information being global, it does not so permit to precisely capture all local shape variations present in the training set. But we think that local shape variations of the object to segment can be accurately and efficiently segmented by boundary-based active contours. Combining shape prior with geodesic active contours, Chen *et al.* have proposed in [25] a variational model composed by a shape term calculated from a shape prior (not probabilist) and by the geodesic active contours term which simultaneously achieves registration and segmentation. Therefore, we firstly propose to extend the segmentation model of Chen *et al.* by integrating the statistical shape model of Leventon *et al.*. We will demonstrate that the proposed variational model is mathematically justified since a solution minimizing the functional exists in the space of functions of bounded variation. Moreover the statistical shape term being in a variational formulation, we will use other segmentation variational terms such as region-based terms in [18, 19] to realize the segmentation. We secondly propose to globally guide the shape prior towards regions of interest in images by using region-based image features based on the Mumford-Shah functional [17, 18]. This additional term increases the robustness of the segmentation model and the speed of convergence.
In section 2, we briefly review some state-of-the-art results which are directly connected to our work. In section 3, we define our new variational model to realize objects segmentation with a prior shape knowledge and derive the system of evolution equations minimizing the proposed energy. Then in section 4, we introduce the Mumford-Shah functional in the framework. We present experimental results to validate the proposed method on 2-D synthetic and real-world images. Finally, we conclude and compare our model to other methods and we show in appendix the existence of a solution for our minimization problems.

2. ACTIVE CONTOUR FAMILIES AND PCA SHAPE MODELING

In this section, we propose to briefly review the three main families of active contours, i.e. the boundary-based, the region-based and the shape-based active contours. We also present the shape model of Leventon *et al.* [22].

2.1. Boundary-Based/Geodesic Active Contours

The first model of boundary-based active contour was proposed by Kass *et al.* [10]. This model locates sharp image intensity variations by deforming a curve C towards the edges of objects. The evolution equation of C is given by the minimization of the energy functional $F(C) = \int_0^1 |C'(p)|^2 dp + \beta \int_0^1 |C''(p)|^2 dp + \lambda \int_0^1 g^2(|\nabla I(C(p))|) dp$ which g is an edge detecting function vanishing at infinity. This segmentation model presents two main drawbacks. Firstly, the functional F depends on the parametrization of the curve C. This means that different parametrizations of the curve give different solutions for the same initial condition. Secondly, this approach does not take into account changes of topology. As a result, the final curve has the same topology as the initial one. To overcome the first limitation, Caselles *et al.* [26] and Kichenassamy *et al.* [27, 28] have proposed a new energy functional which is invariant w.r.t. a new curve parametrization. The new intrinsic energy functional is $F^{GAC}(C) = 2\sqrt{\lambda} \int_0^{L(C)} g(|\nabla I(C(s))|) ds$, where ds is the Euclidean element of length. F^{GAC} is actually a new length obtained by weighting the Euclidean element of length by the function g which contains information regarding the objects boundaries. Caselles *et al.* have also proved in [26] that the final curve is a geodesic in a Riemannian space. This geodesic is computed by the calculus of variations providing the Euler-Lagrange equations of F^{GAC} and the gradient descent method which gives the flow minimizing the functional F^{GAC}: $\partial_t C = (\kappa g - < \nabla g, \mathcal{N} >)\mathcal{N}$, where $\mathcal{N}$ is the unit normal to the curve C and κ is its curvature. To overcome the second limitation, Osher and Sethian proposed the level set method in [11, 5]. The curve C is thus implicitely represented by a level set function φ. Finally, a curve evolution $\partial_t C = F\mathcal{N}$ can be re-written in a level set formulation: $\partial_t \varphi = F|\nabla\varphi|$ which evolution of the curve C coincides with the evolution of the zero level set of φ as shown in [26].

2.2. Region-Based Active Contours

Paragios and Deriche [15, 16] have employed new evolution criteria built from statistics on the regions to segment. Their variational method, called *geodesic active regions*, allows to unify boundary- and region-based statistical knowledge into a single energy functional which is minimized by a set of PDEs.
In [19, 20], a general paradigm for active contours is presented, derived from functionals that include local and global statistical measures of homogeneity for the regions being segmented. Their criteria to minimize have the general form:

$$F^R(\Omega_{in}, \Omega_{out}, C) = \int_C k^b(x)ds + \int_{\Omega_{in}} k^{in}(x, \Omega_{in})d\Omega + \int_{\Omega_{out}} k^{out}(x, \Omega_{out})d\Omega, \quad (1)$$

where Ω^{in}, Ω^{out} are respectively the inner and the outer region of the active contour, k^{in} and k^{out} are the *descriptors* of these regions and k^b is the boundary descriptor. To determine the solution minimizing (1), shape optimization tools [29, 30] are needed to differentiate (1) w.r.t. the domains Ω_{in} and Ω_{out} which evolve in time. Then, the evolution equations of active contours are deduced from the derivative of F^R to minimize as fast as possible F^R. By using the entropy descriptor from [19], the following flow produces very good segmentation results as we can see on Figure 2 (a) and (b).
In [17, 18, 31], a method to solve the Mumford-Shah functional [9] in the context of propagating contours is proposed. The Mumford and Shah's approach to solve the image segmentation problem has been extensively studied (see [4, 7] and [18] for references) but we restrict our attention to the active contours framework. The Mumford-Shah minimization problem is defined as follows:

$$\inf_{u,C} \{F^{MS}(u, C) = \int_\Omega |u - u_0|^2 dx + \mu \int_{\Omega - C} |\nabla u|^2 + \nu \mathcal{H}^{N-1}(C)\}, \quad (2)$$

where u corresponds to an optimal piecewise smooth approximation of an original image u_0, C represents the edges of u and the length of C is given by the (N-1)-dimensional Hausdorff measure $\mathcal{H}^{N-1}(C)$ [2]. Chan and Vese [17, 18] have proposed a model to minimize the functional (2). A piecewise smooth approximation of a given image is computed (which allows image denoising) by minimizing the following functional w.r.t. a level set function φ and two functions u_{in} and u_{out} (we consider here only two regions Ω_{in} and Ω_{out} even if Chan and Vese have solved the complete image partitioning problem):

$$F^{MS}_{CV}(u_{in}, u_{out}, \varphi) = \nu \int_\Omega |\nabla H(\varphi)| + \int_\Omega (|u_{in} - u_0|^2 + \mu |\nabla u_{in}|^2) H(\varphi) dx + \int_\Omega (|u_{out} - u_0|^2 + \mu |\nabla u_{out}|^2) H(-\varphi) dx, \quad (3)$$

where H is the Heaviside function. The evolution equation of the level set function embedding the active contour is as follows:

$$\partial_t \varphi = \delta(\varphi)(\nu\kappa + |u_{out} - u_0|^2 + \mu|\nabla u_{out}|^2 - |u_{in} - u_0|^2 - \mu|\nabla u_{in}|^2). \quad (4)$$

An example of segmentation using this model is given on Figure 2 (c)-(e).

2.3. Shape-Based Active Contours

Leventon *et al.* [22, 32] have developed active contours employing a statistical shape model defined by a PCA over a training set of the structure of interest (see section 2.4). In their approach, the active surface, represented by a level set function, evolves locally based on image gradients and surface curvature like the classical geodesic active contour and globally towards the maximum a posteriori probability (MAP) of position and shape of the prior shape model of the object to be segmented. Moreover, the a posteriori probability of position and shape is maximized at each iteration by an independant optimization process. It has the advantage of providing a segmentation model robust with respect to noise and initial positioning surface but it has also the drawback to loose the nature of a PDE for the surface evolution equation since two independant stages are now necessary to evolve the surface. The evolution equation is the following one:

$$\begin{aligned} u(t+1) &= u(t) + \lambda_1(g(c+\kappa)|\nabla u(t)| + < \nabla u(t), \nabla g >) \\ &+ \lambda_2(u^\star(t) - u(t)). \end{aligned} \quad (5)$$

where $u^\star$ is the MAP final position and shape of the prior shape model. The second term of the right-hand side of (5) represents the classical term of the geodesic active contour. And the third term evolves the shape of the active surface towards the one given by the MAP estimation.
Tsai *et al.* [33, 34] have integrated the statistical model of shape of Leventon *et al.* in the reduced version of the Mumford-Shah functional proposed by Chan et Vese in [17] to segment images containing known object types.
In [35, 25], Chen *et al.* have designed a novel variational model that incorporates prior shape knowledge into geometric/geodesic active contours. Contrary to

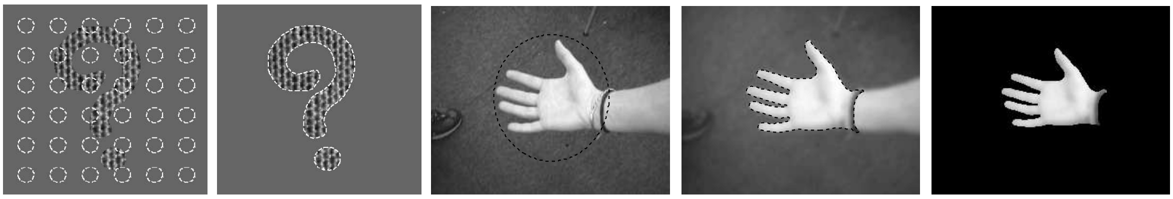

(a) (b) (c) (d) (e)

Fig. 2. Figures (a),(b) show a segmentation using the region-based active contour of Jehan-Besson *et al.*, Figures (c),(d) present a segmentation using the active contour of Chan and Vese based on the Mumford-Shah functional and Figure (e) represents a smooth approximation of the hand.

Leventon's approach, the shape model $C^\star$ of Chen is not a probabilistic one. It is computed by averaging a training set of rigidly registered curves. However, this variational approach has the advantage to mathematically demonstrate the existence of solutions minimizing the following energy functional which is not the case in the Leventon's model. The functional of Chen is:

$$F^S(C,\mu,\theta,T) = \int_0^1 (g(|\nabla I(C(p))|) + \frac{\lambda}{2} d^2(\mu RC(p)+T))|C'(p)|dp, \quad (6)$$

where C is the active contour, (μ,θ,T) are the parameters of a rigid transformation and d is the distance function of $C^\star$, the target shape. This functional is thus minimized when the active contour has captured high image gradients and the shape prior. They have showed the good ability of the model to extract real-world structures in which the complete boundary was either missing or had low resolution and low constrat [35, 25].

Paragios and Rousson in [23, 36] have built a new level set representation of shape from a training set which is able to capture global and local shape variations. They have used it to non-rigidly register two shapes and to segment objects with a modified version of the geodesic active regions.

Finally, Cremers *et al.* [37, 38, 39] have modified the Mumford-Shah functional to incorporate two statistical models of parametric shape in order to efficiently segment known objects in the case of misleading information due to noise, occlusion and strongly cluttered background. Concerning the shape model, they have assumed in [37] that the training shapes form a multivariate Gaussian distribution and they have employed in [38] a nonlinear shape statistic derived from an extension of the kernel PCA.

2.4. The Statistical Shape Model of Leventon et al.

We finish this section by presenting the shape model developed by Leventon *et al.* [22] which we use in our segmentation model. This shape model is computed by the PCA which main advantage is to capture the principal features of a training set while removing redundant information. Cootes et al. [21] have employed successfully this technique to segment different kind of objects. The new idea of Leventon et al. [22] is to apply the PCA not on the parametric geometric curves as Cootes did but on the SDFs of these curves, which are implicit representations. They justified their choice by two facts. The first one is that the SDFs provide a *stronger* tolerance than the parametric curves to slight misalignments during the alignment process of the training data since the values of neighboring pixels are highly correlated in SDFs. The second fact is that this intrinsic shape representation does not constraint to solve the contour point-wise correspondence problem.

From a geometric point of view, the PCA analysis determines the best orthonormal basis $\{\mathbf{e}_1 ... \mathbf{e}_m\}$ of $\mathcal{R}^m$ to represent a set of n points $\{\phi_1 ... \phi_n\}$ in the sense of the least squares fitting [40]. In our work, a SDF ϕ_j is represented by N^q samples (q is the number of dimensions and N the number of samples for each dimension), hence $m = N^q$. In the PCA, a point ϕ_j is represented by the formula: $\phi_j = \overline{\phi} + \sum_{i=1}^m \alpha_{ji}\mathbf{e}_i + R_j = \hat{\phi}_j + R_j$ where $\overline{\phi}$ is the geometric average of $\{\phi_j\}_j$ and R_j is the distance between the point ϕ_j and $\hat{\phi}_j$, the orthogonal projection of the vector ϕ_j into the space spans by the basis $\{\mathbf{e}_i\}_i$.

The PCA aims at finding out the vectors $\{\mathbf{e}_i\}_i$ which minimize the quadratic error $\varepsilon = \sum_{j=1}^n \|R_j\|^2$ under the constraint that these vectors form an orthonormal basis in $\mathcal{R}^m$. These vectors are given by the eigenvectors of the covariance matrix $\mathbf{\Sigma} = \frac{1}{n} M M^\top$ where M is a matrix which column vectors are the n centered training SDF ϕ_j. The vectors $\{\mathbf{e}_i\}_i$ correspond to the principal variation directions of the set of n points. They are the *principal components*. Moreover, the first p principal axes define a reduced p-dimensional vector space in $\mathcal{R}^m$ equivalent to an hyper-plan minimizing the sum of squared distances between this hyperplan and the set of n points. It is important to note that the fitting goodness of this p-D hyperplan in relation to the set of points can be measured in percentage by the formula $\beta = \sum_{k=1}^{p} \lambda_k / \sum_{k=1}^{n} \lambda_k$ where λ_k are the eigenvalues of $\mathbf{\Sigma}$. It is possible to arbitrarly fix the fitting percentage β and represent the data in a sub-vector space of dimension p. In practice, the importance of principal modes of a training set strongly decreases because the training data represent the same class of objects. Thus, only a small number of eigenmodes is useful for our purpose. These p principal components are sorted in a matrix $\mathbf{W}_p$. Thus, the projected data $\hat{\phi}$ in the p-D space of a data ϕ in $\mathcal{R}^m$ is given by the following equations:

$$\begin{cases} \hat{\phi} = \mathbf{W}_p \mathbf{x}_{pca} + \overline{\phi}, \\ \mathbf{x}_{pca} = \mathbf{W}_p^{\top} (\phi - \overline{\phi}), \end{cases} \tag{7}$$

where $\mathbf{x}_{pca}$ is the vector of eigencoefficients. Finally, if we suppose that the probability density funtion (PDF) of the training set is a Gaussian function then the probability distribution of $\hat{\phi}(\mathbf{x}_{pca})$ is

$$P(\hat{\phi}(\mathbf{x}_{pca})) = \frac{1}{(2\pi)^{p/2} |\mathbf{\Lambda}_p|^{1/2}} exp(-\frac{1}{2} \mathbf{x}_{pca}^{\top} \mathbf{\Lambda}_p^{-1} \mathbf{x}_{pca}), \tag{8}$$

where $\mathbf{\Lambda}_p$ is a diagonal matrix containing the first p eigenvalues.

3. A VARIATIONAL MODEL FOR IMAGE SEGMENTATION WITH STATISTICAL SHAPE KNOWLEDGE AND BOUNDARY-BASED INFORMATION

3.1. The Proposed Segmentation Model

In [41], we have formulated a new energy functional which is minimized once the active contour has captured high image gradients and a shape compatible with the statistical model of the object of interest. This functional is actually an extension of the work of Chen *et al* [35, 25] where we have integrated the statistical shape model of Leventon *et al* [22]. The proposed energy to achieve image segmentation with a statistical shape prior is:

$$F_1 = \beta_b F_{boundary}(C) + \beta_s F_{shape}(C, \mathbf{x}_{pca}, \mathbf{x}_T), \tag{9}$$

$$\text{where } F_{boundary} = \oint_0^1 g(|\nabla I(C(q))|) |C'(q)| dq, \tag{10}$$

$$F_{shape} = \oint_0^1 \hat{\phi}^2(\mathbf{x}_{pca}, h_{\mathbf{x}_T}(C(q))) |C'(q)| dq. \tag{11}$$

In these definitions, g is the edge detecting function, $\hat{\phi}$ is a *shape* function provided by the PCA (7) over the training SDFs of the object to segment, $\mathbf{x}_{pca}$ is the vector of PCA eigencoefficients, $h_{\mathbf{x}_T}$ is an element of a group of geometric transformations which $\mathbf{x}_T$ is the vector of parameters, and β_b, β_s are arbitrary positive constants that balance the contributions of the boundary term and the shape term.

3.2. The Shape Term F_{shape}

F_{shape} is a shape-based functional depending on the active contour C, the vector of PCA eigencoefficients $\mathbf{x}_{pca}$ and the vector of geometric transformations $\mathbf{x}_T$. This functional evaluates the shape difference between the contour C and the zero level set $\hat{C}$ of the PCA shape function $\hat{\phi}$. It is an extension of the shape-based term of Chen *et al* [35, 25] where we have integrated the statistical shape model of Leventon *et al* [22]. If we consider a rigid transformation with the scale parameter equal to one, the function $\hat{\phi}^2$ at the point $C(q)$ is equal to

$$\begin{aligned} \hat{\phi}^2(\mathbf{x}_{pca}, h_{\mathbf{x}_T}(C(q))) \simeq \\ \| \hat{C}_{\mathbf{x}_{pca}}(p_{min}) - h_{\mathbf{x}_T}(C(q)) \|_2^2 . \end{aligned} \tag{12}$$

The equality is not strict since the shape function $\hat{\phi}$ is not a SDF as Leventon noticed [22, 32]. However, the PCA applied on registred SDFs of a training set produces shape functions *very close* to a SDF. Figure 3 gives an illustration of the function $\hat{\phi}^2$. If we desire to get a strict equality in Equation (12), we must preserve the shape prior function $\hat{\phi}$ as a SDF. Two solutions are possible, either the shape function is projected in the SDF space by redistancing $\hat{\phi}$ as a SDF or the framework of G. Charpiat *et al.* [24, 42] can be employed to define a mean and principal modes of variation for distance functions by PDEs and using [43] for preserving SDFs.

Finally, F_{shape} is obtained by integrating $\hat{\phi}^2$ along the active contour, which defines the shape similarity measure equivalent to the sum of square differences (SSD). The minimization of F_{shape} allows us to increase the shape similarity between the active contour and the shape model. The functional is minimized with the calculus of variations and the gradient descent methods which provides three flows acting on the curve C, the

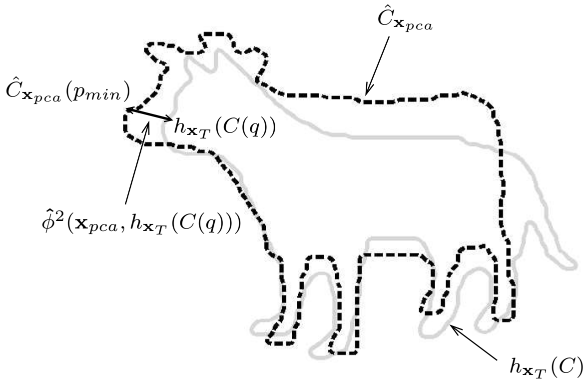

Fig. 3. Interpretation of the function $\hat{\phi}^2(\mathbf{x}_{pca}, h_{\mathbf{x}_T}(C(q)))$: the square shape function at the contour point $C(q)$ is approximatively equal to the square Euclidean distance between the contour point $h_{\mathbf{x}_T}(C(q))$ under a geometric transformation and the closest point $\hat{C}_{\mathbf{x}_{pca}}(p_{min})$ on the zero level set of $\hat{\phi}(\mathbf{x}_{pca})$

vector of eigencoefficients $\mathbf{x}_{pca}$ and the vector of geometric transformations $\mathbf{x}_T$. The flow minimizing F_{shape} w.r.t. the curve C is the classical flow of [26]:

$$\left\{ \begin{array}{l} \partial_t C(t,q) = \\ \quad (\hat{\phi}^2 \kappa - < \nabla \hat{\phi}^2, \mathcal{N} >) \mathcal{N} \text{ in }]0,\infty[\times [0,1], \\ C(0,q) = C_0(q) \text{ in } [0,1]. \end{array} \right. \quad (13)$$

The flows minimizing F_{shape} w.r.t. the vector of eigencoefficients $\mathbf{x}_{pca}$ are:

$$\left\{ \begin{array}{l} d_t \mathbf{x}_{pca}(t) = -2\beta_s \int_0^1 \hat{\phi} \nabla_{\mathbf{x}_{pca}} \hat{\phi}\ |C'| dq \text{ in } \Omega_{pca}, \\ \mathbf{x}_{pca}(t=0) = \mathbf{x}_{pca_0} \text{ in } \Omega_{pca}. \end{array} \right. \quad (14)$$

$$\text{with} \quad \nabla_{\mathbf{x}_{pca}} \hat{\phi} = \left(\begin{array}{c} \mathbf{e}^1_{pca} \\ \vdots \\ \mathbf{e}^p_{pca} \end{array} \right), \quad (15)$$

where $\mathbf{e}^i_{pca}$ the ith principal component of the PCA model, $\Omega_{pca} = [-3\lambda_1, 3\lambda_1] \times ... \times [-3\lambda_p, 3\lambda_p]$ and λ_i is the eigenvalue of the ith principal component. And the flows minimizing F_{shape} w.r.t. the vector of geometric transformations $\mathbf{x}_T$ are:

$$\left\{ \begin{array}{l} d_t \mathbf{x}_T(t) = \\ \quad -2\beta_s \int_0^1 \hat{\phi} < \nabla \hat{\phi}, \nabla_{\mathbf{x}_T} h_{\mathbf{x}_T}(C) > |C'| dp \text{ in } \Omega_T, \\ \mathbf{x}_T(t=0) = \mathbf{x}_{T_0} \text{ in } \Omega_T. \end{array} \right. \quad (16)$$

In (13), (14) and (16), the function $\hat{\phi}$ is evaluated at $(\mathbf{x}_{pca}, h_{\mathbf{x}_T}(C(q))$. In our work, we have considered the rigid and the affine transformations:

$$h_{\mathbf{x}^r_T} : x \rightarrow h_{(s,\theta,T)}(x) = sR_\theta x + T, \quad (17)$$

$$h_{\mathbf{x}^a_T} : x \rightarrow h_{(s_x,s_y,\theta,T,s_h)}(x) = R_{sc} R_\theta R_{sh} x + T, \quad (18)$$

$$\text{where } R_{sc} = \left(\begin{array}{cc} s_x & 0 \\ 0 & s_y \end{array} \right),$$

$$R_\theta = \left(\begin{array}{cc} \cos\theta & \sin\theta \\ -\sin\theta & \cos\theta \end{array} \right) \text{ and } R_{sh} = \left(\begin{array}{cc} 1 & s_h \\ 0 & 1 \end{array} \right). \quad (19)$$

The vector of rigid transformations $\mathbf{x}^r_T$ is composed of a scale parameter s, an angle of rotation θ and a vector of translations T and the vector of affine transformations $\mathbf{x}^a_T$ is composed of two scale parameters s_x in x-direction and s_y in y-direction, an angle of rotation θ, a shearing parameter s_h and a vector of translations T. $\mathbf{x}^r_T$ lies thus in $\Omega_T = [0,256] \times [-\pi,\pi] \times [-256,256]^2$ and $\mathbf{x}^a_T$ in $\Omega_T = [0,256]^2 \times [-\pi,\pi] \times [-256,256]^2 \times [-128,128]$. In our implementation, we have considered the same value for both scale parameters, i.e. $s_x = s_y = s$.

As a consequence, the gradient term $\nabla_{\mathbf{x}_T} h_{\mathbf{x}_T}$ in (16) depending on geometric transformations is

$$\nabla_{\mathbf{x}^r_T} h_{\mathbf{x}^r_T}(x) = \left(\begin{array}{l} \frac{\partial h_{\mathbf{x}^r_T}}{\partial s}(x) = R_\theta x \\ \frac{\partial h_{\mathbf{x}^r_T}}{\partial \theta}(x) = s\partial_\theta R_\theta x \\ \frac{\partial h_{\mathbf{x}^r_T}}{\partial T}(x) = \mathbf{1} \end{array} \right) \text{ and} \quad (20)$$

$$\nabla_{\mathbf{x}^a_T} h_{\mathbf{x}^a_T}(x) = \left(\begin{array}{l} \frac{\partial h_{\mathbf{x}^a_T}}{\partial s}(x) = R_\theta R_{sh} x \\ \frac{\partial h_{\mathbf{x}^a_T}}{\partial \theta}(x) = s\partial_\theta R_\theta R_{sh} x \\ \frac{\partial h_{\mathbf{x}^a_T}}{\partial s_h}(x) = sR_\theta \partial_{s_h} R_{sh} x \\ \frac{\partial h_{\mathbf{x}^a_T}}{\partial T}(x) = \mathbf{1} \end{array} \right). \quad (21)$$

Next, we re-write the previous equations in a variational level set formulation as presented in [44, 25]. The level set approach of [44], rather than [26, 27, 28], is used for proving existence of solutions minimizing our energy functional. The level set formulations of the functional (11) and the system of equations (13), (14) and (16) are:

$$F_{shape} = \int_\Omega \hat{\phi}^2(\mathbf{x}_{pca}, h_{\mathbf{x}_T}(x)) |\nabla\varphi| \delta(\varphi) d\Omega. \quad (22)$$

$$\left\{ \begin{array}{l} \partial_t \varphi(t,x) = \\ \quad \left(\hat{\phi}^2 \kappa |\nabla\varphi| - < \nabla\hat{\phi}^2, \nabla\varphi > \right) \delta(\varphi) \text{ in }]0,\infty[\times \Omega, \\ \varphi(0,x) = \varphi_0(x) \text{ in } \Omega, \\ \frac{\delta(\varphi)}{|\nabla\varphi|} \partial_{\mathcal{N}} \varphi = 0 \text{ on } \partial\Omega. \end{array} \right. \quad (23)$$

$$\left\{ \begin{array}{l} d_t \mathbf{x}_{pca}(t) = \\ -2\beta_s \int_\Omega \hat{\phi} \nabla_{\mathbf{x}_{pca}} \hat{\phi} |\nabla\varphi| \delta(\varphi) d\Omega \text{ in } \Omega_{pca}, \\ \mathbf{x}_{pca}(t=0) = \mathbf{x}_{pca_0} \text{ in } \Omega_{pca}. \end{array} \right. \quad (24)$$

$$\left\{ \begin{array}{l} d_t \mathbf{x}_T(t) = \\ -2\beta_s \int_\Omega \hat{\phi} < \nabla\hat{\phi}, \nabla_{\mathbf{x}_T} h_{\mathbf{x}_T} > |\nabla\varphi| \delta(\varphi) d\Omega \text{ in } \Omega_T, \\ \mathbf{x}_T(t=0) = \mathbf{x}_{T_0} \text{ in } \Omega_T. \end{array} \right. \quad (25)$$

The steady-state solution of equation (23) allows us to match the active contour shape into any shape prior provided by the PCA model. This shape matching has two main advantages. Firstly, it is independant of the contour parametrization because of the intrinsic level set representation. That means that the contour point-wise correspondance problem is replaced by a grid point-wise intensity correspondance which is easier to solve. Secondly, it is more accurate than parametrized shape matching since the degree of deformation of level set functions is higher. Figure 4 shows two curves matching.

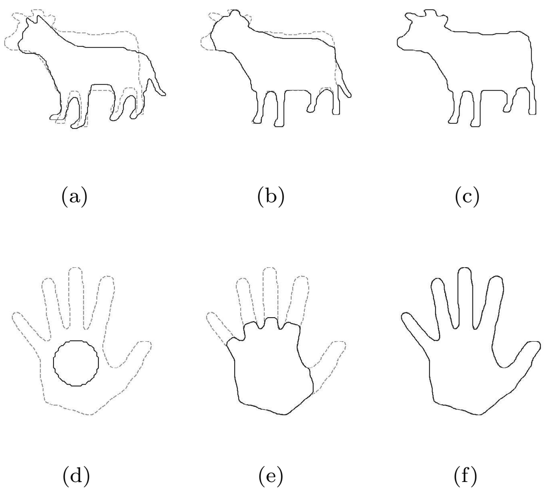

Fig. 4. Minimization of F_{shape} with the flow (23), $\mathbf{x}_T$ and $\mathbf{x}_{pca}$ being fixed. Active contour is in solid line and the shape prior in dotted line. Figures (a)-(c) show the matching of a cat (initial active contour) into a cow (shape prior). Figures (d)-(f) present the matching of a circle into a hand.

The steady-state solution of the system of equations (24) and (25) allow us to register the zero level set of the shape function with the active contour. This means that we can use the shape function of variables $\mathbf{x}_{pca}$ and $\mathbf{x}_T$ as a registration functional that permits to register the shape prior onto any shape represented by the active contour. Figures 5 and 6 shows some affine registrations and Figure 7 presents an affine and shape registration.

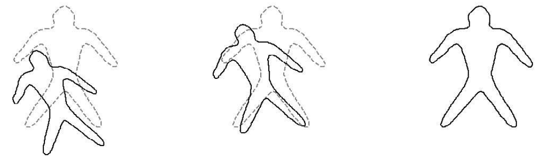

Fig. 5. Minimization of F_{shape} with the flow (25), ϕ and $\mathbf{x}_{pca}$ being fixed. Figures present the affine registration of a prior shape in solid line into an active contour in dotted line.

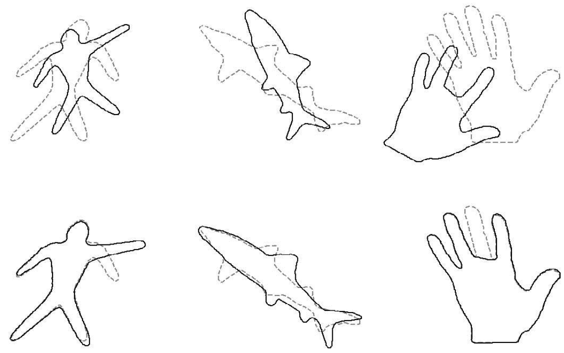

Fig. 6. Minimization of F_{shape} with the flow (25), ϕ and $\mathbf{x}_{pca}$ being fixed. Each column presents the affine registration of a prior shape in solid line into an active contour in dotted line. The first row shows the initial positions of shapes and the second row the registered shapes. This registration process works with shapes having different local structures and with missing information.

3.3. Evolution Equations Minimizing The Functional F_1

In this section, we compute the system of coupled equations which steady-state solution gives a minimum of the proposed functional (9) to realize the segmentation process with prior shape. We directly write the system of flows in the Eulerian formulation. If we define

$$f(x, \mathbf{x}_{pca}, \mathbf{x}_T) \equiv \beta_b g(|\nabla I(x)|) + \beta_s \hat{\phi}^2(\mathbf{x}_{pca}, h_{\mathbf{x}_T}(x)), \quad (26)$$

then, we have

$$F_1 = \int_\Omega f(x, \mathbf{x}_{pca}, \mathbf{x}_T)|\nabla\varphi|\delta(\varphi)d\Omega. \quad (27)$$

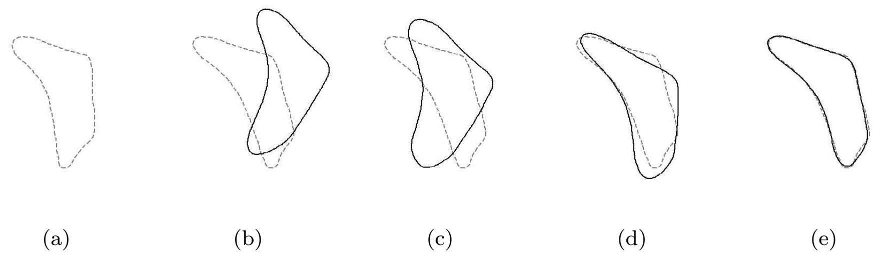

Fig. 7. Minimization of F_{shape} with flows (24) and (25), ϕ being fixed. Figure (a) presents a left ventricle taken from a training set of left ventricles. Figure (b) shows in dotted line the left ventricle of Fig.(a) changed by an affine transformation and an initial shape prior in solid line. Figures (c-d) represent the evolution of the registration process according to the geometric trnsformations $\mathbf{x}_T$ and the PCA model $\mathbf{x}_{pca}$. Finally, figure (e) displays the registration of both shapes.

The system of flows is thus

$$\begin{cases} \partial_t\varphi(t,x) = \\ \quad (f\kappa|\nabla\varphi| - < \nabla f, \nabla\varphi >)\,\delta(\varphi) \text{ in }]0,\infty[\times\Omega, \\ \varphi(0,x) = \varphi_0(x) \text{ in } \Omega, \\ \frac{\delta(\varphi)}{|\nabla\varphi|}\partial_{\mathcal{N}}\varphi = 0 \text{ on } \partial\Omega. \end{cases} \tag{28}$$

$$\begin{cases} d_t\mathbf{x}_{pca}(t) = \\ \quad -2\beta_s \int_\Omega \hat{\phi}\nabla_{\mathbf{x}_{pca}}\hat{\phi}|\nabla\varphi|\delta(\varphi)d\Omega \text{ in } \Omega_{pca}, \\ \mathbf{x}_{pca}(t=0) = \mathbf{x}_{pca_0} \text{ in } \Omega_{pca}. \end{cases} \tag{29}$$

$$\begin{cases} d_t\mathbf{x}_T(t) = \\ \quad -2\beta_s \int_\Omega \hat{\phi} < \nabla\hat{\phi}, \nabla_{\mathbf{x}_T}h_{\mathbf{x}_T} > |\nabla\varphi|\delta(\varphi)d\Omega \text{ in } \Omega_T, \\ \mathbf{x}_T(t=0) = \mathbf{x}_{T_0} \text{ in } \Omega_T. \end{cases} \tag{30}$$

We prove in appendix that a solution (at least) minimizing our energy functional F_1 exists in the space of functions of bounded variation. This allows to say that our segmentation model is well-posed.

3.4. Implementation issues

Concerning the PCA, the first stage consists on aligning training curves of the object of interest. This is realized with the shape similarity measure of Chen *et al.* [35, 25]:

$$a(C_1, C_j^{new}) = \text{aera of } (A_1 \cup C_j^{new} - A_1 \cap A_j^{new}) \quad \text{for } 2 \le j \le n, \tag{31}$$

where A_1 and A_j^{new} denote the interior regions of the curves C_1 and C_j^{new}, $C_j^{new} = s_j R_{\theta_j} C_j + T_j$ and n is the number of training curves. C_1 and C_j are aligned when the measure a is minimized with the appropriate values $s_j^\star$, $\theta_j^\star$ and $T_j^\star$. These values are computed with a genetic algorithm [45] as optimization process. And the SDFs of the aligned training curves are generated with the fast algorithm described in [46].

The second stage of the PCA realizes the singular values decomposition with the code provided by the Numerical Recipies [47] on the matrix $\mathbf{\Sigma}^{dual} = \frac{1}{n}M^\top M$ (see section 2.4 for notations) to extract the n eigenvalues $\mathbf{e}_{pca}^{i,dual}$ and the eigenvectors $\lambda_{pca}^{i,dual}$. The PCA performed on $\mathbf{\Sigma}^{dual}$ rather than $\mathbf{\Sigma}$ gives fast and accurate results and the eigenvectors $\mathbf{e}_{pca}^i$ and the eigenvalues λ_{pca}^i are given by $\mathbf{e}_{pca}^i = M\mathbf{e}_{pca}^{i,dual}$ and $\lambda_{pca}^i = \lambda_{pca}^{i,dual}$.

Concerning the evolution equations (28), (29) and (30), they are numerically solved by iterating the following stages until convergence is reached:

1. Computation of the shape function $\hat{\phi}(\mathbf{x}_{pca}, \mathbf{x}_T)$ by using the formula (7) and by performing the rigid and affine transformations (scaling, rotation, translations and shearing) with the polynomial B-splines interpolation method [48].
2. The term $\nabla_{\mathbf{x}_{pca}}\hat{\phi}$ is given by the PCA model, see equation (15), $\nabla\hat{\phi}$ uses a central difference sheme and $\nabla_{\mathbf{x}_T}h_{\mathbf{x}_T}$ is computed according to equations (20) and (21).
3. Discretization of terms $|\nabla\phi|$ and $< \nabla f, \nabla\phi >$ with the Osher-Sethian's numerical flux function [11, 5, 25]. Computation of curvature uses standard central difference schemes. And we have approximated the Dirac function δ and the Heaviside function H by slightly regularized versions like in [44, 25].
4. Calculation of the temporal derivative is done with a forward difference approximation.
5. Redistancing the level set function every iteration with the fast marching method of Adalsteinsson

and Sethian [49].

3.5. Experimental Results

3.5.1. Synthetic Images

We have tested our model in 2-D synthetic images with a training set of ellipses. We have generated a set of 30 ellipses by changing the size of a principal axis with a Gaussian PDF. Then we have applied the PCA on the training SDFs of ellipses and we have obtained one principal component that fits at 98% the set of 30 SDFs of ellipses. Figure 8 shows the aligned training ellipses and the shape function corresponding to the mean and the eigenmode of variation of the training set.

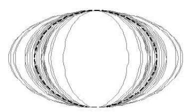

(a)

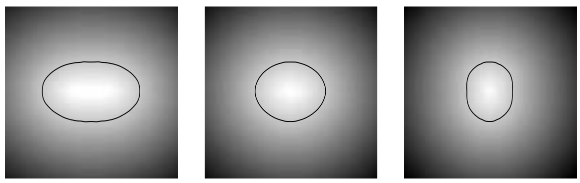

(b) -2λ (c) Mean (d) 2λ

Fig. 8. Figure (a) presents the 30 aligned training ellipses, figure (c) shows the mean value and (d),(e) the eigenmode of variation of ellipses. The zero level set of the shape function $\hat{\phi}$ is plotted in solid dark line.

In the first experiment, we want to segment an ellipse which is partially cut. Figure 9 presents the classical active contour *without* a shape prior and figure 10 *with* a shape prior taking $\beta_b = 1$, $\beta_s = 1/3$ and $\Delta t = 0.6$. We can see on figure 10 that the active contour has captured high image gradients and a shape belonging to the statistical model which best fits the ellipse in the image.
In the second experiment, we want to segment an ellipse which is partially occluded by a vertical bar and which present irregular boundaries. Figure 11 presents the classical active contour *without* a shape prior and figure 12 *with* a shape prior choosing $\beta_b = 1$, $\beta_s = 1/3$ and $\Delta t = 0.6$.

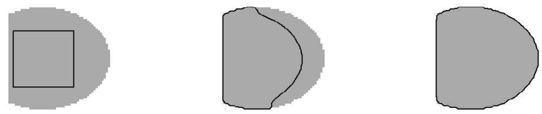

Fig. 9. Evolution of an active contour *without* a shape prior.

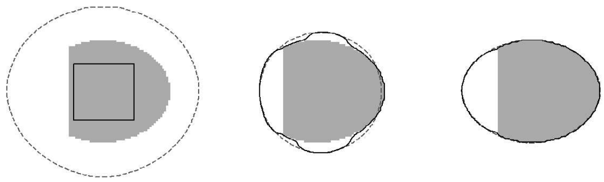

Fig. 10. Evolution of an active contour (in solid line) *with* a shape prior (in dotted line).

We have showed with the two previous synthetic examples that our shape-based active contour model can segment objects with missing information, occlusion and local shape deformations.

3.5.2. Real Images

We have also experimented our model in 2-D natural images. We have employed 2-D medical images. We have used 45 2-D images of left ventricles to build our statistical shape model. These 2-D images are extracted from several slices of T1-Weighted Magnetic Resonance images of healthy voluntaries (Figure 13). We have applied the PCA and we have obtained three principal components that fit at 88.2% the set of 45 SDFs of ventricles. Figure 14 shows the aligned training ventricles and the shape function corresponding to the mean and the three main eigenmodes of variation of the training set.
In this experiment, we want to segment the left ventricle. Figure 15 presents the evolving active contour *without* a shape prior and figure 16 *with* a shape prior taking $\beta_b = 1$, $\beta_s = 2$ and $\Delta t = 0.4$. We observe on Figure 16 that the active contour has well captured the left ventricle whereas *the initial contour was around the two ventricles* on Figure 16(a). This segmentation result could not be obtained without a shape prior with the same initial contour as we can observe on Figure 15. The segmentation model has also provided the shape of the statistical model which best fits the ventricle ly-

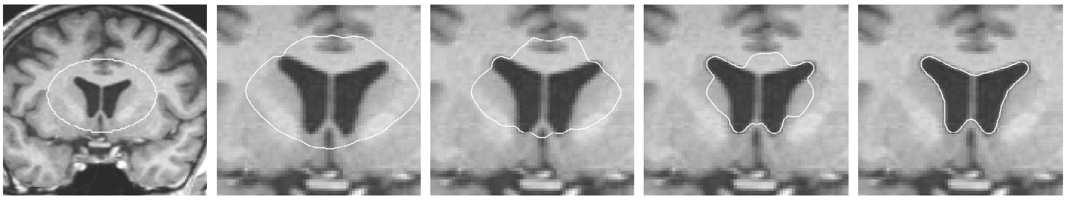

(a) (b) (c) (d) (e)

Fig. 15. Evolution of an active contour *without* a shape constraint.

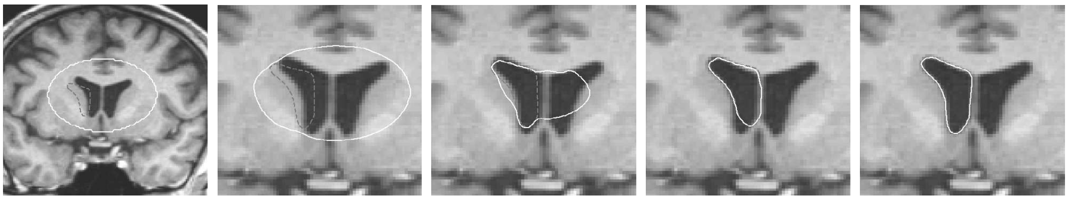

(a) (b) (c) (d) (e)

Fig. 16. Evolution of an active contour (in solid line) *with* a shape prior (in dotted line).

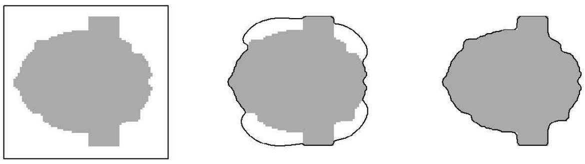

Fig. 11. Evolution of an active contour *without* a shape prior.

ing in the image and its associated probability given by equation (8).

3.6. Using Other Segmentation Models

In the framework of variational models and PDEs, it is possible to use other segmentation models such as region-based segmentation methods developped in section 2.2. The easiest way is to linearly combine energy functionals or PDEs directly. For examples, if we want to use the statistiscal measures of homogeneity introduced by Jehan-Besson *et al.* [19], the new functional to minimize is $F^{new} = F_1(C, \mathbf{x}_{pca}, \mathbf{x}_T) + \lambda_R F^R(\Omega_{in}, \Omega_{out}, C)$ or if we want to employ the Mumford-Shah approach of Chan and Vese [17, 18], the energy is $F^{new} = F_1(C, \mathbf{x}_{pca}, \mathbf{x}_T) + \lambda_{MS} F^{MS}_{CV}(u_{in}, u_{out}, C)$. The PDE minimizing F^{new} is obviously a linear combination of PDEs minimizing each term of F^{new}.

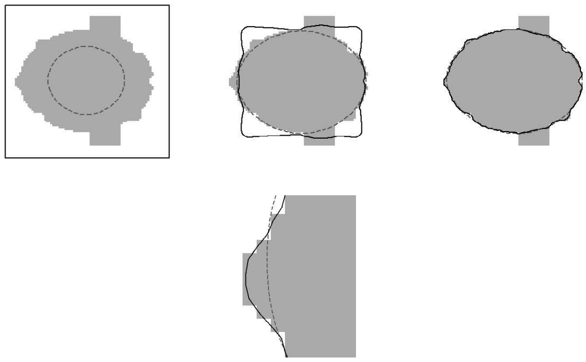

Fig. 12. The first row presents the evolution of an active contour (in solid line) *with* a shape prior (in dotted line). The second row is a zoom on the left point of the ellipse to show that the active contour is able to segment local structures even with the shape prior.

In our work, we have decided to integrate a region-based segmentation model into the shape prior rather than the active contour. The main raison is based on the observation of Figures 15 and 16 where we want to

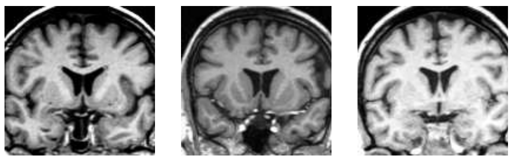

Fig. 13. Three T1-Weighted Magnetic Resonance images of brain.

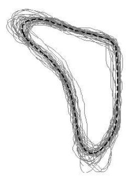

(a)

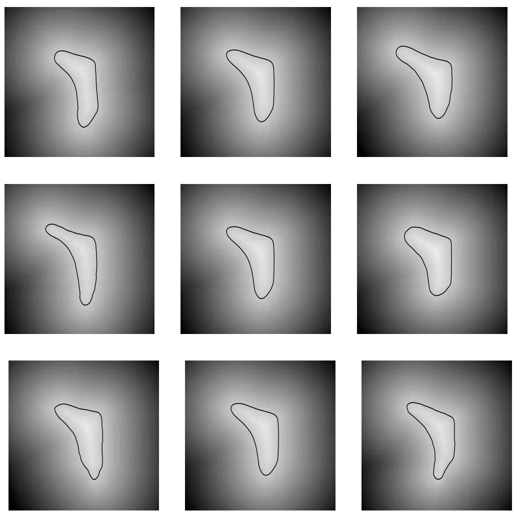

Fig. 14. Figure (a) presents the 45 aligned training ventricles, the middle column is the mean value and each row presents an eigenmode of variation of ventricles. The zero level set of the shape function $\hat{\phi}$ is plotted in solid dark line.

segment the left ventricle with an initial contour around both ventricles. If the region homogeneity criterium is employed on the active contour, the region-based force on the right ventricle is opposed to the shape-based force since the shape prior pulls the active contour inside whereas the region-based term constraints the active contour to stay on the edges of the right ventricle to keep a homogeneous region. Of course, we want to avoid this situation. A solution is to put the region homogeneity criterium into the shape prior to drive it towards a smooth intensity region which has the shape of interest.

In the next section, we develop the introduction of the region-based criterium into our segmentation model.

4. INTRODUCTION OF REGION HOMOGENEITY FEATURES IN THE SEGMENTATION MODEL

4.1. A Functional Based on the Mumford-Shah's Model

In this section, we employ the Mumford-Shah functional (2) to segment a smooth region which shape is a priori known by the PCA model. We have modified the model of Chan and Vese [18], presented in section 2.2, to integrate the prior shape model and the geometric transformations:

$$\begin{aligned} F_{region}(\mathbf{x}_{pca}, \mathbf{x}_T, u_{in}, u_{out}) = \oint_{\hat{C}(\mathbf{x}_{pca},\mathbf{x}_T)} ds + \\ \int_{\Omega_{in}(\mathbf{x}_{pca},\mathbf{x}_T)} (|u_0 - u_{in}|^2 + \mu|\nabla u_{in}|^2) d\Omega + \\ \int_{\Omega_{out}(\mathbf{x}_{pca},\mathbf{x}_T)} (|u_0 - u_{out}|^2 + \mu|\nabla u_{out}|^2) d\Omega, \end{aligned} \quad (32)$$

where the curve $\hat{C}$ is the zero level set of the shape function $\hat{\phi}$ computed by the PCA on a training set of the object of interest. The function $\hat{\phi}$ allows to define an image partioning into two regions Ω_{in} and Ω_{out} which common boundary is $\hat{C}$:

$$\begin{cases} \Omega_{in}(\mathbf{x}_{pca}, \mathbf{x}_T) = \{x \in \Omega \mid \hat{\phi}(x, \mathbf{x}_{pca}, \mathbf{x}_T) > 0\}, \\ \Omega_{out}(\mathbf{x}_{pca}, \mathbf{x}_T) = \{x \in \Omega \mid \hat{\phi}(x, \mathbf{x}_{pca}, \mathbf{x}_T) < 0\}, \\ \hat{C}(\mathbf{x}_{pca}, \mathbf{x}_T) = \{x \in \Omega \mid \hat{\phi}(x, \mathbf{x}_{pca}, \mathbf{x}_T) = 0\}. \end{cases} \quad (33)$$

The segmentation problem defined in equation (3), section 2.2, depending on the active contour represented by φ is now changed into a segmentation model depending on the vector $\mathbf{x}_{pca}$ of shape eigencoefficients and the vector $\mathbf{x}_T$ of geometric transformations. In our work, we have cancelled the smoothing term, $\oint_{\hat{C}} ds$, since shapes generated by the PCA are enough smooth. We re-write the functional F_{region} with the shape function $\hat{\phi}$:

$$\begin{aligned} F_{region}(\mathbf{x}_{pca}, \mathbf{x}_T, u_{in}, u_{out}) = \\ \int_\Omega \Theta_{in} H(\hat{\phi}(\mathbf{x}_{pca}, \mathbf{x}_T) d\Omega + \\ \int_\Omega \Theta_{out} H(-\hat{\phi}(\mathbf{x}_{pca}, \mathbf{x}_T) d\Omega, \end{aligned} \quad (34)$$

where $\Theta_r = |u_0 - u_r|^2 + \mu|\nabla u_r|^2$ and $r = in$ or out. The modified Mumford-Shah's functional is minimized using gradient flows for $\mathbf{x}_{pca}$ and $\mathbf{x}_T$ and the Euler-Lagrange equations for u_{in} and u_{out}. Thus, the flows minimizing (34) w.r.t. $\mathbf{x}$ which can be either $\mathbf{x}_T$ or $\mathbf{x}_{pca}$ are:

$$d_t\mathbf{x} = \int_\Omega (\Theta_{in} - \Theta_{out}) \frac{\partial\hat{\phi}}{\partial\mathbf{x}} \delta(\hat{\phi}) d\Omega, \qquad (35)$$

$$\text{with} \quad \begin{cases} \frac{\partial\hat{\phi}}{\partial\mathbf{x}_T} =< \nabla\hat{\phi}, \nabla_{\mathbf{x}_T} h_{\mathbf{x}_T} >, \\ \frac{\partial\hat{\phi}}{\partial\mathbf{x}_{pca}} = \nabla_{\mathbf{x}_{pca}}\hat{\phi}. \end{cases}$$

And the Euler-Lagrange equations of (34) w.r.t. u_{in} and u_{out} are:

$$\begin{cases} u_{in} - u_0 = \mu\Delta u_{in} \text{ in } \{\hat{\phi} > 0\}, \\ u_{out} - u_0 = \mu\Delta u_{out} \text{ in } \{\hat{\phi} < 0\}. \end{cases} \qquad (36)$$

We have noticed that another segmentation method based on the Mumford-Shah functional and the PCA model of Leventon *et al.* have already been proposed by Tsai *et al.* [34] *but* for a reduced version of the Mumford-Shah model. They actually have employed the piecewise constant case of the Mumford-Shah functional, proposed by Chan and Vese [17], whereas we have used the piecewise smooth case [18]. Our model gives better segmentation results since it avoids possible intensity bias due to the inhomogeneity of the outside region, i.e. the background, with respect to the inside region, the object of interest.

4.2. Implementation Issues

Minimization of F_{region}, with equations (35) and (36), is numerically done by iterating the following stages until convergence is reached:

1. Computation of the shape function $\hat{\phi}(\mathbf{x}_{pca}, \mathbf{x}_T)$ using formula (7) and polynomial B-splines interpolation [48] for spatial transformations. We have approximated the Dirac function δ and the Heaviside function H as in [44, 25].

2. Discretization of $\frac{\partial\hat{\phi}}{\partial\mathbf{x}}$ using a central difference sheme for $\nabla\hat{\phi}$, equations (20), (21) for $\nabla_{\mathbf{x}_T} h_{\mathbf{x}_T}$ and equation (15) for $\nabla_{\mathbf{x}_{pca}}\hat{\phi}$.

3. Functions u_{in} and u_{out} are computed by a Gaussian filtering in $\{\hat{\phi} > 0\}$ and $\{\hat{\phi} < 0\}$ since $u_r = u_0 + \mu\Delta u_r = G(\sqrt{2\mu}) * u_0 + \mathcal{O}(\mu)$, where r is *in* or *out* and G is the Gaussian function. Then Θ_r are estimated.

4. Computation of the temporal derivative is done with a forward difference approximation.

4.3. Experimental Results

We have tested the functional F_{region} by segmenting several ellipses in different situations presented on Figure 17. This segmentation model is so able to process missing information, occlusions and noise. However, this segmentation method can not handle local structure deformations as we see on Figure 17(f) with the ellipse which presents irregular boundaries. The model hasn't captured local edge variations since it works with *global* shapes provided by the PCA. If we want to segment the entire boundary, with local structures, we must combine this global approach with local method as the classical edge-based active contour.
We have also employed this model for segmenting the left ventricle in brain as we can see on Figure 18.

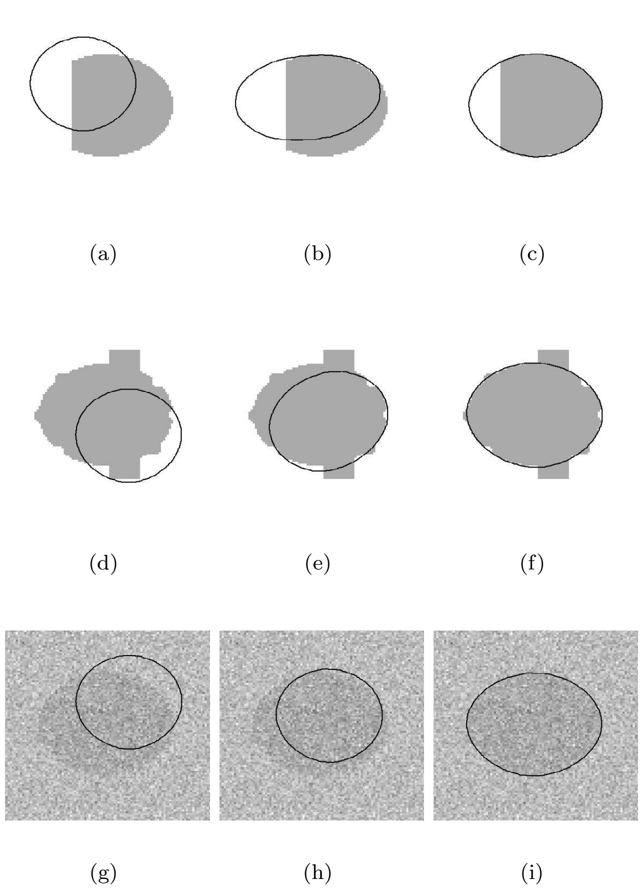

Fig. 17. Minimization of F_{region} with the flow (35) and the equation (36). The first row presents the evolution of the segmentation process of an ellipse partially cut. The second row is the segmentation of an occluded ellipse. And the third row shows the segmentation of a noisy ellipse.

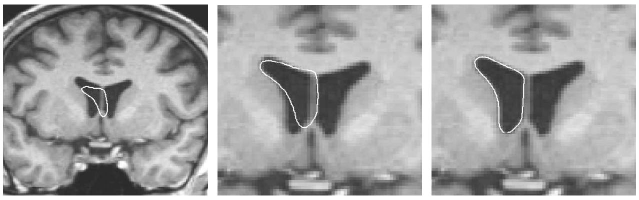

Fig. 18. Segmentation of the left ventricle by minimizing F_{region} with the flow (35) and the equation (36).

4.4. Combining Boundary-based, Shape-based and Region-based Functionals

In sections 3.1 and 3.2, we have defined a shape-based functional F_{shape} which evaluates the similarity between the active contour shape and the shape prior given by the PCA of the object to segment. In this section, we have formulated a region-based functional F_{region} which allows us to drive globally the shape prior towards a homogeneous intensity region. We now linearly combine these two types of functionals with the boundary-based functional $F_{boundary}$, which captures edges, to get a functional for segmenting objects with a geometric shape prior and local and global image information:

$$F_2 = \beta_b F_{boundary}(C) + \beta_s F_{shape}(C, \mathbf{x}_{pca}, \mathbf{x}_T) + \beta_r F_{region}(\mathbf{x}_{pca}, \mathbf{x}_T, u_{in}, u_{out}). \quad (37)$$

4.5. Evolution Equations Minimizing The Functional F_2

In this section, we compute the system of coupled gradient flows in the implicit (Eulerian) formulation of [44, 25] which steady-state solution provides the minimimum of the proposed functional (37):

$$F_2 = \int_\Omega f(x, \mathbf{x}_{pca}, \mathbf{x}_T)|\nabla\varphi|\delta(\varphi)d\Omega + \beta_r \int_\Omega \left(\Theta_{in} H(\hat{\phi}(\mathbf{x}_{pca}, \mathbf{x}_T)) + \Theta_{out} H(-\hat{\phi})\right) d\Omega. \quad (38)$$

$$\begin{cases} \partial_t \varphi(t,x) = \\ \quad (f\kappa|\nabla\varphi| - < \nabla f, \nabla\varphi >)\,\delta(\varphi) \text{ in }]0,\infty[\times\Omega, \\ \varphi(0,x) = \varphi_0(x) \text{ in } \Omega, \\ \frac{\delta(\varphi)}{|\nabla\varphi|}\partial_{\mathcal{N}}\varphi = 0 \text{ on } \partial\Omega. \end{cases} \quad (39)$$

$$\begin{cases} d_t \mathbf{x}_{pca}(t) = -2\int_\Omega \nabla_{\mathbf{x}_{pca}} \hat{\phi}(2\beta_s\hat{\phi}|\nabla\varphi|\delta(\varphi) + \\ \quad \beta_r(\Theta_{in} - \Theta_{out})\delta(\hat{\phi}))d\Omega \text{ in } \Omega_{pca}, \\ \mathbf{x}_{pca}(t=0) = \mathbf{x}_{pca_0} \text{ in } \Omega_{pca}. \end{cases} \quad (40)$$

$$\begin{cases} d_t \mathbf{x}_T(t) = -2\int_\Omega < \nabla\hat{\phi}, \nabla_{\mathbf{x}_T} g_{\mathbf{x}_T} > \\ \quad (2\beta_s\hat{\phi}|\nabla\varphi|\delta(\varphi) + \\ \quad \beta_r(\Theta_{in} - \Theta_{out})\delta(\hat{\phi}))d\Omega \text{ in } \Omega_T, \\ \mathbf{x}_T(t=0) = \mathbf{x}_{T_0} \text{ in } \Omega_T. \end{cases} \quad (41)$$

$$\begin{cases} u_{in} - u_0 = \mu\Delta u_{in} \text{ in } \{\hat{\phi} > 0\} \cap \Omega, \\ u_{out} - u_0 = \mu\Delta u_{out} \text{ in } \{\hat{\phi} < 0\} \cap \Omega. \end{cases} \quad (42)$$

Existence of a solution (at least) minimizing our energy functional F_2 is shown in appendix.

4.6. Experimental Results

We have employed our complete segmentation model for segmenting the left ventricle, Figure 19 taking $\beta_b = 1$, $\beta_s = 2$, $\beta_r = 0.1$, $\mu = 3$ and $\Delta t = 0.4$. Even if we get the same final result than in section 3.5.2, i.e. without the region-based term, the evolution process is different. Firstly, it is more robust to noise and initial position of the shape prior. And secondly, the convergence is faster since more image information is taken into account during the segmentation process. Observe the difference between the Figure 16(d) and Figure 19(d). In the first figure, the boundary-based force is weaker than the shape-based force, so the active contour does not stay on the border and go inside the ventricle. Whereas in the second figure, the region-based information allows us to drive the shape prior directly towards the correct homogeneous region.

5. DISCUSSION

In this paper, we have proposed a new variational model to solve the segmentation problem of objects of interest using local and global image information and a prior geometric shape given by the statistical model of PCA. We have seen that active contours, which result from the minimization of the energy functional (37) is able to capture high image gradients, a shape of the statistical model which best fits the segmented object providing

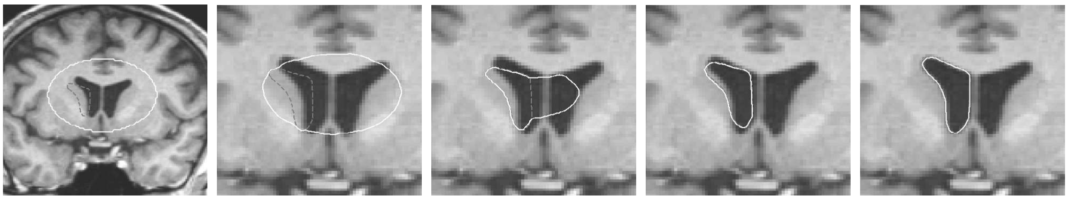

(a) (b) (c) (d) (e)

Fig. 19. Segmentation of the left ventricle by minimizing the functional F_2 with flows (39), (40), (41) and equation (42).

robustness against missing information due to cluttering, occlusion and gaps, and a homogeneous intensity region. Experimental results have showed that the ability of active contours to segment any natural structure is preserved thanks to the implicit/level set formulation of active contour. This is one of the main advantage of choosing this contour representation rather than explicit/parametrized representation which provides less freedom of deformation. The introduction of the Mumford-Shah functional, which implicitly means that only smooth intensity objects are segmented, has increased the robustness of the model w.r.t. initial conditions, noise and complex background. Our model can also take advantages of other variational segmentation models such as [19, 18].

As we previously said, the proposed model is partially an extension of the model of Chen *et al.* [25] where we have introduced the statistical shape model of Leventon *et al.* [22]. One can wonder why to use the model of Chen to compute the vector $\mathbf{x}_T$ of spatial geometric transformations and the vector $\mathbf{x}_{pca}$ of eigencoefficients since the model of Leventon already does by MAP estimation. The key idea of this choice is to use the correct mathematical formulation of Chen to solve the segmentation problem. Indeed, our proposed model is mathematically justified since we prove the existence of a solution in the space of function of bounded variation (in appendix).

In [23], Paragios and Rousson have proposed a level set representation of shape from a training set which is able to capture global and local shape variations. Their shape model generates more different shapes than the PCA but the shape vector $\mathbf{x}_{pca}$, which is composed by only p unknown variables in our approach, is replaced by a local deformation field to evaluate on a δ-band around the zero level set of the shape function.

In our segmentation model like in [22, 25, 23], the geometric shape model is introduced through a shape registration between the prior shape and the active contour. Thus the proposed segmentation/registration model computes the vector of spatial transformations wich can be used with other segmentation results to solve the important image registration problem. For example in [25, 50], image registration is employed in order to align time series images to minimize the effect of motion on the fMRI signal. Our model also computes the shape vector $\mathbf{x}_{pca}$ which gives the probability that the final shape function $\hat{\phi}(\mathbf{x}_{pca})$ belongs to the class of the training set thanks to the equation (8). In pratice, we have noticed that the optimization procedure, i.e. the gradient descent method, applied on $\mathbf{x}_T$ and $\mathbf{x}_{pca}$ strongly depends on discretization steps to reach the correct solution in a reasonable time.

In [37, 38], Cremers *et al.* define two shape statistical energies invariant w.r.t. rigid transformation and shape parameters. In [37], they use the assumption that the PDF of the training set is a Gaussian function which leads to the Mahalanobis distance by taking the log-function of the PDF. Cremers *et al.* use parametrized contours in their model but the Mahalanobis distance can also be applied to contours represented by level set functions as proposed in [51]. Estimating or not the registration parameters $\mathbf{x}_T$ and $\mathbf{x}_{pca}$ depends on two questions: does the current application need pose and shape parameters and are affine or non-rigid transformations necessary? If the answer is yes for one of these questions, the estimation of pose ans shape parameters will be imperative.

The PCA aims at defining two important quantities, the mean and the variance, which are used to estimate the PDF of the training set of the object to segment. These two quantities can define a uniform PDF and also a Gaussian PDF, which is generally preferred. But the Gaussian function to represent the true underlying PDF of the training set can be very inappropriate (in presence of tumors in T1-WMR images for example). Future work is naturally based on the extension of the PCA to more elaborated techniques such as non-

parametric models.
Finally, the proposed model can capture only one object which is limited since we lose the powerful property of the level set approach which can segment several objects simultaneously. A first solution would consist on associating structures by coupling the evolution equations.

Appendix: Existence Of Solution For Our Minimization Problems

This section deals with the mathematical studies of

$$\min_{\varphi,\mathbf{x}_{pca},\mathbf{x}_T}\{F_1 = \int_\Omega \left(\beta_b g(x) + \beta_s \hat{\phi}^2(x,\mathbf{x}_{pca},\mathbf{x}_T)\right)|\nabla H(\varphi)|\} \quad (43)$$

and

$$\min_{\varphi,\mathbf{x}_{pca},\mathbf{x}_T,u_{in},u_{out}}\{F_2 = \int_\Omega \left(\beta_b g(x) + \beta_s \hat{\phi}^2(x,\mathbf{x}_{pca},\mathbf{x}_T)\right)|\nabla H(\varphi)| + \beta_r F_{region}(\mathbf{x}_{pca},\mathbf{x}_T,u_{in},u_{out})\}. \quad (44)$$

We follow the demonstration of Chen *et al.* in [35, 25] and Vese and Chan [52] to prove the existence of a minimizer for our proposed minimization problems using the direct method of the calculus of variations and compactness theorems on the space of functions with bounded variation.
The minimization problem is considered among characteristic functions χ_E of sets $E = \{x \in \Omega | \varphi(x) \geq 0\}$ with bounded variation. The vector of PCA eigencoefficients $\mathbf{x}_{pca} = (\mathbf{x}_{pca_1},...,\mathbf{x}_{pca_p})$ and the vector of geometric transformations $\mathbf{x}_T = (s,\theta,T,s_h)$ are respectively defined on Ω_{pca} and Ω_T. Functions u_{in} and u_{out} are in $C^1(\Omega)$ since u_r is a smoothed version of the original image u_0 ($u_r = u_0 + \mu\Delta u_r$ is the discretized version of the linear heat diffusion equation $\partial_t u_r = \Delta u_r$ with $u_r(0) = u_0$).

We remind some definitions and theorems introduced in Evans [2], Giusti [3], Chen [35, 25], Chan and Vese [52] and Ambrosio [53].

Definition 1: Let $\Omega \subset \mathbb{R}^N$ be an open set and let $f \in L^1(\Omega)$. The total variation norm of f is defined by

$$TV(f) = \int_\Omega |\nabla f| = \sup_{\phi\in\Phi}\left\{\int_\Omega f(x)\mathrm{div}\ \phi(x)\right\}, \quad (45)$$

$$\text{where} \quad \Phi = \left\{\phi \in C_0^1(\Omega,\mathbb{R}^N) |\ |\phi(x)| \geq 1, \text{on } \Omega\right\}. \quad (46)$$

Definition 2: A function $f \in L^1(\Omega)$ is said to have bounded variation in Ω if its distributional derivate satisfies $TV(f) < \infty$. We define $BV(\Omega)$ as the space of all functions in $L^1(\Omega)$ with bounded variation. The space $BV(\Omega)$ is a Banach space, endowed with the norm:

$$\|f\|_{BV(\Omega)} = \|f\|_{L^1(\Omega)} + TV(f). \quad (47)$$

Theorem 1 *A measurable subset E of $\mathbb{R}^N$ has finite perimeter in Ω if and only if the characteristic function $\chi_E \in BV(\Omega)$. We have $per_\Omega(E) = TV(\chi_E) = \int_\Omega |\nabla\chi_E| < \infty$.*

Definition 3: Let $\Omega \subset \mathbb{R}^N$ be an open set and let $f \in L^1(\Omega)$ and $\alpha(x)$ be positive valued continuous and bounded functions on Ω. The weighted total variation norm of f is defined by

$$TV_\alpha(f) = \int_\Omega \alpha(x)|\nabla f| = \sup_{\phi\in\Phi_\alpha}\left\{\int_\Omega f(x)\mathrm{div}\ \phi(x)\right\}, \quad (48)$$

$$\text{where} \quad \Phi_\alpha = \left\{\phi \in C_0^1(\Omega,\mathbb{R}^N) |\ |\phi(x)| \geq \alpha(x), \text{on } \Omega\right\}. \quad (49)$$

If a function f has a finite weighted total variation norm in Ω then it also belongs to $BV(\Omega)$.

Theorem 2 *Let $\Omega \subset \mathbb{R}^N$ be an open set with a Lipschity boundary. If $\{f_n\}_{n\geq1}$ is a bounded sequence in $BV(\Omega)$, then there exist a subsequence $\{f_{n_j}\}$ of $\{f_n\}$ and a function $f \in BV(\Omega)$, such that $f_{n_j} \to f$ strongly in $L^1(\Omega)$ and*

$$TV(f) \leq \liminf_{n_j\to\infty} TV(f_{n_j}). \quad (50)$$

The following theorem is a generalization of the **main theorem** of Chen [35, 25].

Theorem 3 *Let $\Omega \subset \mathbb{R}^N$ be an open set with a Lipschity boundary. If $\{f_n\}_{n\geq1}$ is a bounded sequence in $BV(\Omega)$ and if $\{\alpha_n\}_{n\geq1}$ is a sequence of positive valued continuous functions which uniformly converges to α on Ω, then there exist subsequences $\{f_{n_j}\}$ of $\{f_n\}$ and a function $f \in BV(\Omega)$ such that $f_{n_j} \to f$ strongly in $L^1(\Omega)$ and*

$$TV_\alpha(f) \leq \liminf_{n_j\to\infty} TV_{\alpha_{n_j}}(f_{n_j}). \quad (51)$$

Theorem 4 *Let Ω be a bounded and open subset of $\mathbb{R}^N$ and I be a given image with $I \in L^\infty(\Omega)$. The minimization problem (43) re-writes in the following form*

$$\min_{\chi_E,\mathbf{x}_{pca},\mathbf{x}_T}\{F_1 = \int_\Omega \left(\beta_b g(x) + \beta_s \hat{\phi}^2(x,\mathbf{x}_{pca},\mathbf{x}_T)\right)|\nabla\chi_E|\} \quad (52)$$

has a solution $\chi_E \in BV(\Omega)$, $\mathbf{x}_{pca} \in \Omega_{pca}$ and $\mathbf{x}_T \in \Omega_T$.

Proof: We use the direct method of the calculus of variations:
(A) Let $\{\chi_{E n}, \mathbf{x}_{pca_n}, \mathbf{x}_{T n}\}_{n\geq 1}$ be a minimizing sequence of (52), i.e.

$$\lim_{n\to\infty} F_1(\chi_{E n}, \mathbf{x}_{pca_n}, \mathbf{x}_{T n}) = \inf_{\chi_E, \mathbf{x}_{pca}, \mathbf{x}_T} F_1(\chi_E, \mathbf{x}_{pca}, \mathbf{x}_T). \tag{53}$$

(B) Since $\chi_{E n}$ is a sequence of characteristic functions of E_n, then $\chi_{E n}(x) \in \{0, 1\}$ - a.e. in Ω. There exists $M > 0$ such that $\|\chi_{E n}\|_{L^1(\Omega)} \leq M$, $\forall n \geq 1$. Therefore, $\chi_{E n}$ is a uniformly bounded sequence on $BV(\Omega)$.
Since $\{\mathbf{x}_{pca}\}_n$ and $\{\mathbf{x}_{T_n}\}_n$ are bounded sequences on compact spaces Ω_T and Ω_{pca}, there exist subsequences which converge to limits $\mathbf{x}_{pca}$ and $\mathbf{x}_T$.
The integrant $f(x, \mathbf{x}_{pca}, \mathbf{x}_T) = \beta_b g + \beta_s \hat{\phi}^2$ is positive and bounded because both terms g and $\hat{\phi}^2$ are bounded on Ω. Since the PCA is applied on continuous functions (SDFs) then functions $\hat{\phi}$ and f are continuous functions and $f_m(\mathbf{x}) = f(\mathbf{x}, \mathbf{x}_{T_m}, \mathbf{x}_{\alpha_m})$ uniformly converges to f on Ω.
By theorem 3, there exists a subsequence of $\chi_{E n}$ which converges to a function χ_E strongly in $L^1(\Omega)$.
(C) Moreover , theorem 3 also states that

$$\int_\Omega f|\nabla\chi_E| \leq \liminf_{n_j\to\infty} \int_\Omega f_{n j}|\nabla\chi_{E_{n j}}|, \tag{54}$$

this implies that $\chi_E \in BV(\Omega)$ and χ_E, $\mathbf{x}_{pca}$, $\mathbf{x}_T$ are minimizers of (52).

Definition 4: A function $f \in BV(\Omega)$ is a special function of bounded variation if its distributional derivative is given by

$$|Df| = TV(f) + \int_{\Omega\cap S_f} J_f d\mathcal{H}^{N-1}, \tag{55}$$

where J_f is the jump part defined on the set of points S_f and $\mathcal{H}^{N-1}$ as in section 2.2 is the (N-1)-dimensional Hausdorff measure. The space of special functions of bounded variation $SBV(\Omega)$ is a Banach space, endowed with the norm:

$$\|f\|_{SBV(\Omega)} = \|f\|_{L^1(\Omega)} + |Df|. \tag{56}$$

Theorem 5 *Let Ω be a bounded and open subset of $\mathbb{R}^N$ and I be a given image with $I \in L^\infty(\Omega)$. The minimization problem (44) re-writes in the following form*

$$\begin{aligned} \mathop{inf}_{\chi_E, \mathbf{x}_{pca}, \mathbf{x}_T, u_{in}, u_{out}} &\{F_2 = \\ &\textstyle\int_\Omega \left(\beta_b g(x) + \beta_s \hat{\phi}^2(x, \mathbf{x}_{pca}, \mathbf{x}_T)\right) |\nabla\chi_E| + \\ &\beta_r F_{region}(\mathbf{x}_{pca}, \mathbf{x}_T, u_{in}, u_{out})\} \end{aligned} \tag{57}$$

has a solution $\chi_E \in BV(\Omega)$, $\mathbf{x}_{pca} \in \Omega_{pca}$, $\mathbf{x}_T \in \Omega_T$ and u_{in}, $u_{out} \in C^1(\Omega)$.

Proof: For (B), the same method of Theorem 4 is used and for (C), we employ the demonstration of Vese and Chan [52]:
(A) Let $\{\chi_{E n}, \mathbf{x}_{pca_n}, \mathbf{x}_{T_n}, u_{in_n}, u_{out_n}\}_{n\geq 1}$ be a minimizing sequence of (57), i.e.

$$\lim_{n\to\infty} F_2(\chi_{E n}, \mathbf{x}_{pca_n}, \mathbf{x}_{T_n}, u_{in_n}, u_{out_n}) = \inf_{\chi_E, \mathbf{x}_{pca}, \mathbf{x}_T, u_{in}, u_{out}} F_2(\chi_E, \mathbf{x}_{pca}, \mathbf{x}_T, u_{in}, u_{out}). \tag{58}$$

(B) for the same reasons than in Theorem 4 and with Theorem 3, we have

$$\int_\Omega f|\nabla\chi_E| \leq \liminf_{n_j\to\infty} \int_\Omega f_{n j}|\nabla\chi_{E_{n j}}|. \tag{59}$$

(C) In the region-based functional (34)

$$F_{region}(\mathbf{x}_{pca}, \mathbf{x}_T, u_{in}, u_{out}) = \int_\Omega (\Theta_{in} H(\hat{\phi}(\mathbf{x}_{pca}, \mathbf{x}_T)) + \Theta_{out} H(-\hat{\phi})) d\Omega, \tag{60}$$

the function $H(\hat{\phi}(\mathbf{x}_{pca}, \mathbf{x}_T))$ is a characteristic function χ_G of sets $G = \{x \in \Omega | \hat{\phi}(x) \geq 0\}$. So we have

$$F_{region}(\mathbf{x}_{pca}, \mathbf{x}_T, u_{in}, u_{out}) = \int_\Omega (\Theta_{in} \chi_G(\mathbf{x}_{pca}, \mathbf{x}_T)) + \Theta_{out}(1 - \chi_G)) d\Omega \tag{61}$$

and we can define the function $u = u_{in}\chi_G + u_{out}(1 - \chi_G)$. The minimizing sequence of (57) implies

$$\lim_{n\to\infty} F_{region}(\mathbf{x}_{pca_n}, \mathbf{x}_{T_n}, u_{in_n}, u_{out_n}) = \inf_{\mathbf{x}_{pca}, \mathbf{x}_T, u_{in}, u_{out}} F_{region}(\mathbf{x}_{pca}, \mathbf{x}_T, u_{in}, u_{out}). \tag{62}$$

Since the function χ_G continuously depends on variables $\mathbf{x}_{pca}$ and $\mathbf{x}_T$, we have $\chi_G(\mathbf{x}_{pca_n}, \mathbf{x}_{T_n}) = \chi_{G n}$ and $u_n = u_{in_n}\chi_{G n} + u_{out_n}(1 - \chi_{G n})$. According to Ambrosio's lemna [53], we can deduce that there is a $u \in SBV(\Omega)$, such that a subsequence u_{n_j} converges to u a.e. in $BV - w*$ and

$$F_{region}(\mathbf{x}_{pca}, \mathbf{x}_T, u_{in}, u_{out}) = F_{region}(u) \leq \liminf_{n_j\to\infty} F_{region}(u_{n_j}), \tag{63}$$

which means that u is a minimizer of F_{region}. Then, combining (59) and (63), χ_E, $\mathbf{x}_{pca}$, $\mathbf{x}_T$, u_{in} and u_{out} are minimizers of (57).

A. REFERENCES

[1] M. Crandall, H. Ishi, and P. Lions, "Users' guide to viscosity solutions of second order partial differential equations," *Bulletin of the American Mathematic Society*, vol. 27(1), pp. 1–69, 1992.

[2] L. Evans and R. Gariepy, *Measure Theory and Fine Properties of Functions*. Studies in advanced Mathematics, CRC Press, 1992.

[3] E. Giusti, *Minimal Surfaces and Functions of Bounded Variation*. Birkhauser, Basel, 1985.

[4] J. Morel and S. Solimini, *Variational Methods in Image Segmentation*. Progress in Nonlinear Differential Equations and Their Applications, 1995.

[5] J. Sethian, *Level Set Methods and Fast Marching Methods: Evolving Interfaces in Computational Geometry, Fluid Mechanisms, Computer Vision, and Material Sciences.* Cambridge University Press, 1999.

[6] G. Sapiro, *Geometric Partial Differential Equations and Image Processing*. Cambridge University Press, 2001.

[7] G. Aubert and P. Kornprobst, *Mathematical Problems in Image Processing: Partial Differential Equations and the Calculus of Variations*, vol. 147. Springer, 2001.

[8] S. Osher and N. Paragios, *Geometric Level Set Methods in Imaging, Vision and Graphics*. Springer Verlag, 2003.

[9] D. Mumford and J. Shah, "Boundary detection by minimizing functionals," in *International Conference on Computer Vision and Pattern Recognition*, pp. 22–26, IEEE, 1985.

[10] M. Kass, A. Witkin, and D. Terzopoulos, "Snakes: Active contour models," *International Journal of Computer Vision*, pp. 321–331, 1987.

[11] S. Osher and J. Sethian, "Fronts propagating with curvature-dependent speed: Algorithms based on hamilton-jacobi formulations," *Journal of Computational Physics*, vol. 79(1), no. 12-49, 1988.

[12] A. Yezzi, S. Kichenassamy, A. Kumar, P. Olver, and A. Tannenbaum, "A geometric snake model for segmentation of medical imagery," *IEEE Transactions on Medical Imaging*, vol. 16(2), pp. 199–209, 1997.

[13] R. Malladi, R. Kimmel, D. Adalsteinsson, G. Sapiro, V. Caselles, and J. Sethian, "A geometric approach to segmentation and analysis of 3d medical images," in *Mathematical Methods in Biomedical Image Analysis Workshop*, 1996.

[14] L. Jonasson, P. Hagmann, X. Bresson, R. Meuli, O. Cuisenaire, and J. Thiran, "White matter mapping in dt-mri using geometric flows," in *9th EUROCAST conference on Computer Aided Systems Theory*, 2003.

[15] N. Paragios and R. Deriche, "Geodesic active contours and level sets for the detection and tracking of moving objects," *IEEE Transactions on Pattern Analysis and Machine Intelligence*, vol. 22, no. 3, pp. 266–280, 2000.

[16] N. Paragios and R. Deriche, "Coupled geodesic active regions for image segmentation: A level set approach," in *European Conference of Computer Vision, 224-240*, pp. 224–240, 2000.

[17] T. Chan and L. Vese, "Active contours without edges," *IEEE Transactions on Image Processing*, vol. 10(2), pp. 266–277, 2001.

[18] T. Chan and L. Vese, "A multiphase level set framework for image segmentation using the mumford and shah model," *International Journal of Computer Vision*, vol. 50(3), pp. 271–293, 2002.

[19] S. Jehan-Besson, M. Barlaud, and G. Aubert, "Dream2s: Deformable regions driven by an eulerian accurate minimization method for image and video segmentation," *Technical Report RR 2001-14, Laboratoire I3S*, 2001.

[20] G. Aubert, M. Barlaud, O. Faugeras, and S. Jehan-Besson, "Image segmentation using active contours: calculus of variations of shape gradients," *Research Report RR 4483, INRIA*, July 2002.

[21] T. Cootes and C. Taylor, "Statistical models of appearance for computer vision, technical report, university of manchester," 1999.

[22] M. Leventon, W. Grimson, and O. Faugeras, "Statistical shape influence in geodesic active contours," in *International Conference of Computer Vision and Pattern Recognition*, pp. 316–323, 2000.

[23] N. Paragios, M. Rousson, and V. Ramesh, "Non-rigid registration using distance functions," *Journal of Computer Vision and Image Understanding*, vol. 89, pp. 142–165, 2003.

[24] G. Charpiat, O. Faugeras, and R. Keriven, "Shape metrics, warping and statistics," in *International Conference on Image Processing*, pp. 627–630, 2003.

[25] Y. Chen, H. Tagare, S. Thiruvenkadam, F. Huang, D. Wilson, K. Gopinath, R. Briggsand, and E. Geiser, "Using prior shapes in geometric active contours in a variational framework," *International Journal of Computer Vision*, vol. 50(3), pp. 315–328, 2002.

[26] V. Caselles, R. Kimmel, and G. Sapiro, "Geodesic active contours," *International Journal of Computer Vision*, vol. 22(1), pp. 61–79, 1997.

[27] S. Kichenassamy, A. Kumar, P. Olver, A. Tannenbaum, and A. Yezzi, "Gradient flows and geometric active contour models," in *International Conference on Computer Vision*, pp. 810–815, IEEE, June 1995.

[28] S. Kichenassamy, A. Kumar, P. Olver, A. Tannenbaum, and A. Yezzi, "Conformal curvature flows: From phase transitions to active vision," in *Archive for Rational Mechanics and Analysis*, vol. 134, pp. 275–301, 1996.

[29] M. Delfour and J. Zolésio, *Shapes and Geometries: Analysis, Differential Calculus, and Optimization*. Advances in Design and Control 4, SIAM, 2001.

[30] J. Sokolowski and J. Zolésio, *Introduction to shape optimization : Shape sensitivity analysis*. Volume 16 of Springer series in computational mathematics, Springer-Verlag, 1992.

[31] A. Tsai, J. Yezzi, and A. Willsky, "Curve evolution implementation of the mumford-shah functional for image segmentation, denoising, interpolation and magnification," *IEEE Transactions on Image Processing*, vol. 10(8), pp. 1169–1186, 2001.

[32] M. Leventon, "Statistical models for medical image analysis, ph.d thesis," 2000.

[33] A. Tsai, A. Yezzi, W. Wells, C. Tempany, D. Tucker, A. Fan, W. Grimson, and A. Willsky, "Model-based curve evolution techniques for image segmentation," in *Conference on computer vision and pattern recognition*, pp. 463–468, 2001.

[34] A. Tsai, A. Yezzi, W. Wells, C. Tempany, D. Tucker, A. Fan, W. Grimson, and A. Willsky, "A shape-based approach to the segmentation of medical imagery using level sets," *IEEE Transactions on Medical Imaging*, vol. 22(2), pp. 137–154, 2003.

[35] Y. Chen, S. Thiruvenkadam, H. Tagare, F. Huang, D. Wilson, and E. Geiser, "On the incorporation of shape priors into geometric active contours," in *Workshop on Variational and Level Set Methods in Computer Vision*, pp. 145–152, 2001.

[36] N. Paragios and M. Rousson, "Shape priors for level set representations," in *European Conference in Computer Vision, Copenhagen, Denmark*, 2002.

[37] D. Cremers, F. Tischhäuser, J. Weickert, and C. Schnörr, "Diffusion snakes: Introducing statistical shape knowledge into the mumford-shah functional," *International Journal of Computer Vision*, vol. 50(3), pp. 295–313, 2002.

[38] D. Cremers, T. Kohlberger, and C. Schnorr, "Nonlinear shape statistics in mumford-shah based segmentation," in *European Conference on Computer Vision*, pp. 93–108, 2002.

[39] D.Cremers, "Statistical shape knowledge in variational image segmentation, ph.d thesis," 2003.

[40] L. Younes, "Modèles statistiques d'images, cours dea."

[41] X. Bresson, P. Vandergheynst, and J. Thiran, "A priori information in image segmentation: Energy functional based on shape statistical model and image information," in *International Conference on Image Processing*, pp. 425–428, 2003.

[42] G. Charpiat, O. Faugeras, and R. Keriven, "Approximations of shape metrics and application to shape warping and empirical shape statistics, inria tr-4820," 2003.

[43] J. Gomes and O. D. Faugeras, "Reconciling distance functions and level sets," in *Scale-Space Theories in Computer Vision*, pp. 70–81, 1999.

[44] H. Zhao, T. Chan, B. Merriman, and S. Osher, "A variational level set approach to multiphase motion," *Journal of Computational Physics*, vol. 127, pp. 179–195, 1996.

[45] L. Davis, *Handbook of Genetic Algorithms*. Van Nostrand, 1991.

[46] O. Cuisenaire and B. Macq, "Fast euclidean distance transformations by propagation using multiple neighbourhoods," *Journal of CVIU*, vol. 76(2), pp. 163–172, 1999.

[47] *Numerical Recipies in C++ and C*. Cambridge University Press.

[48] M. Unser, "Splines: A perfect fit for signal and image processing," *IEEE Signal Processing Magazine*, vol. 16(6), pp. 22–38, 1999.

[49] D. Adalsteinsson and J. Sethian, "A fast level set method for propagating interfaces," *Journal of Computational Physics*, vol. 118, pp. 269–277, 1995.

[50] B. Biswal and J. Hyde, "Contour-based registration technique to differentiate between task-activated and head motion-induced signal variations in fmri," *Magnetic Resonance in Medecine*, vol. 38(3), pp. 470–476, 1997.

[51] J. Yang and J. Duncan, "3d image segmentation of deformable objects with shape-appearance joint prior models," in *Medical Image Computing and Computer-Assisted Intervention*, pp. 573–580, 2003.

[52] L. Vese and T. Chan, "A multiphase level set framework for image segmentation using the mumford and shah model, ucla cam report 01-25," 2001.

[53] L. Ambrosio, "A compactness theorem for a new class of functions of bounded variation," *Bolletino Della Unione Matematica Italiana*, vol. VII(4), pp. 857–881, 1989.